ACS APPLIED MATERIALS & INTERFACES

Research Article

Cite This: ACS Appl. Mater. Interfaces 2019, 11, 17968−17978

www.acsami.org

Photo-Atomic Layer Etching of GaAs/AlGaAs Nanoheterostructures

Mohammad R. Aziziyan, Hemant Sharma, and Jan J. Dubowski*

Laboratory for Quantum Semiconductors and Photon-based BioNanotechnology, Interdisciplinary Institute for Technological Innovation (3IT), CNRS UMI-3463, Department of Electrical and Computer Engineering, Université de Sherbrooke, 3000, boul. de l'Université, Sherbrooke, Québec J1K 0A5, Canada

Supporting Information

ABSTRACT: Photo-atomic layer etching (photo-ALE) of GaAs and AlGaAs semiconductors was investigated in deionized H_2O and aqueous solution of NH_4OH under weak excitation conditions ($P \approx 20$ mW/cm^2). The process is based on digital photocorrosion in a processed solution and a negligible corrosion during the light-off phase employed for dissolution of the photocorrosion products. An inductively coupled plasma mass spectroscopy (ICP-MS) analysis revealed that photo-ALE of GaAs in an aqueous solution of NH_4OH proceeds linearly with the number of reaction cycles, typically at ∼0.1 nm/cycle, and with the light-off phase as short as 22 s sufficient to entirely dissolve the photocorrosion products generated during a 3 s irradiation. In agreement with the ICP-MS data, the constant photo-ALE rates in NH_4OH were also demonstrated in situ with the photoluminescence measurements. Our results suggest that the congruent decomposition of III−V materials and the etching of deep structures with atomic layer resolution could be facilitated by switching in situ between different etching environments.

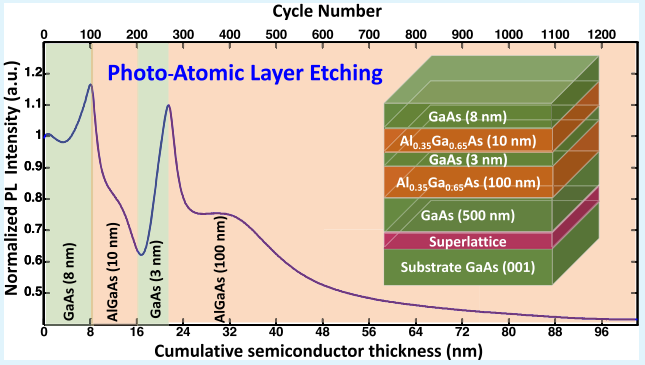

KEYWORDS: *atomic layer etching, compound semiconductors, GaAs/AlGaAs nanoheterostructures, photoluminescence, digital photocorrosion*

1. INTRODUCTION

The unique electronic and optoelectronic properties of GaAs make it attractive for the fabrication of high electron mobility transistors, metal−semiconductor field-effect transistors, and a variety of quantum effect devices.[1−3] The nearly identical lattice constants of GaAs and $Al_{0.35}Ga_{0.65}As$ allowed fabrication of flexibly engineered heterostructures with modulated band gaps, and the two-dimensional electron gas at the interface of such materials was investigated, for example, for tunable plasmonic band gap structure devices.[4] The fabrication of damage-free and stoichiometric surfaces of materials with an atomic depth resolution is of high importance to nanofabrication techniques delivering advanced III−V low-dimensional nanostructures.[5,6] However, the ability to fabricate stoichiometric surfaces of etched GaAs, AlGaAs, and other III−V semiconductors represents a significant challenge. For instance, it has been demonstrated that ion beam-assisted etching consumes at least 10 nm of wet-etched GaAs to produce a stoichiometric surface,[7] rendering this approach unsuitable for the fabrication of devices with atomic depth resolution. Reactive ion beam etching was used for dry etching of GaAs and AlGaAs, and despite fabricating relatively smooth surfaces,[8] ion-induced surface damage appeared unavoidable.[9] To address this problem, GaAs chlorine radical etching without ion bombardment was proposed, although etching rates between 3 nm/min and 10 μm/min were possible only when samples were heated in the range of 300−400 °C.[10] In an electron beam excited plasma system, the surface of GaAs was bombarded sequentially using Ar ions in the presence of Cl_2 or Cl. However, it was reported that accumulation of Cl on GaAs could passivate the surface and suppress the etch rate for the Cl_2 feed time over ∼0.9 s.[11] Maki and Ehrlich proposed bilayer etching of GaAs using a low-pressure Cl_2 chamber to induce a chemical reaction and a 193 nm laser radiation to remove the products of reaction.[12] Although this technique is in principle similar to the Cl_2 etching of GaAs by means of an ion beam, it has been argued that it was the application of low-fluence laser photons that made possible the production of high-quality surfaces.[12,13] In that context, etching with near monolayer depth resolution, also known as digital etching or atomic layer etching (ALE) of semiconductors, has been studied for almost 3 decades now,[14] with some recent works reporting the ALE of zinc oxide[15] and thermal-ALE of aluminum oxide,[16] titanium nitride,[17] silicon,[18] tungsten,[19,20] or silicon dioxide,[21] all aiming at replacing the continuous etching processes that inevitably produce low-quality surfaces.

DeSalvo et al. carried out a two-phase wet chemical digital etching of GaAs surfaces based on the application of a self-limited oxidation reaction.[22] Light-assisted etching of III−V semiconductors has been investigated by Ruberto et al. who

Received: February 7, 2019
Accepted: April 23, 2019
Published: April 23, 2019

DOI: 10.1021/acsami.9b02079
ACS Appl. Mater. Interfaces 2019, 11, 17968−17978

reported microscale photoetching of GaAs and InP using an argon ion laser delivering a 257 nm radiation of power density ranging from 10 mW/cm^2 to 10 kW/cm^2.[23] The etch rates achieved with this technique, ranging between 0.5 mm/min[23] and 2.8 μm/min,[24] were obtained by controlling the potential of a sample immersed in an electrolyte and/or employing a secondary light beam.[25] Fink and Osgood used this approach for the photoetching of GaAs/AlGaAs heterostructures illuminated by a halogen lamp delivering up to 250 mW/cm^2 of optical power density.[26] By measuring current density variation, these authors reported etch rates of ~0.5 μm/min for GaAs and ~0.4 μm/min for AlGaAs. To monitor the process, they took advantage of current density oscillations during the etching of GaAs/AlGaAs interfaces and demonstrated the resolution of a GaAs/AlGaAs interface. Although attaching an ohmic side contact to the sample enhanced the sensitivity of this technique, the demonstration of a layer-by-layer etching was not possible.

The approach common to the previously investigated ALE and digital etching methods concerns the requirement of physically different environments for surface oxidation (vacuum, atmospheric environment, etching liquid) and for the removal of surface oxides (etching liquid or vacuum). In Table S1 (see the Supporting Information), we compared some advantages and disadvantages of digital etching methods of GaAs and GaAs/AlGaAs microstructures investigated in the literature. Note that the photoetching experiments reported by Ruberto et al.[23] and Fink and Osgood[26] did not allow for the resolution of more than three GaAs/AlGaAs interfaces because of a poor depth resolution. The method discussed by Hennessy et al.[27] is based on self-oxidation in an atmospheric environment, which makes it prohibitively slow for industrial applications. Recently, Lin et al.[28] reported on digital etching of InP based on native oxide formation through exposure to oxygen plasma. The products of oxidation are removed in an aqueous solution of H_2SO_4, and etch rates at ~0.9 nm/cycle were reported. The major inconvenience of this approach is that it requires transporting processed samples from plasma producing hardware to a liquid etching environment.

The foregoing discussion stresses that contrary to deposition techniques, advanced methods capable of a comparable controllability and providing accuracy of III−V materials removal have not yet been developed, primarily because of the lack of the universal process as well as diagnostics for in situ monitoring of digital etching processes.[22,29,30]

We have recently demonstrated that so-called digital photocorrosion (DIP) of GaAs/AlGaAs nanoheterostructures could be monitored with photoluminescence (PL) emitted by such nanoheterostructures.[31,32] The sensitivity of DIP to the external perturbations induced by electrically charged molecules allowed the detection of the presence of negatively charged bacteria immobilized in the vicinity of the GaAs/AlGaAs nanoheterostructure surfaces,[31,33] as well as the monitoring of bacterial response to antibiotics in an H_2O environment.[34] This concept has also been investigated for post-growth diagnostics of interface locations in PL-emitting quantum wells,[35] with the possibility of extending it to nanoheterostructures with no PL emission by measuring the open-circuit potential of the photocorroding semiconductor surface.[36] Along with the progress of research in this newly discovered area, it is compelling to understand the mechanisms of photoinduced material removal and formation of stoichiometric surfaces that would be of particular importance to the development of ALE of III−V materials and fabrication of advanced nanoheterostructure devices.

In this paper, inductively coupled plasma mass spectrometry (ICP-MS) was employed for a systematic analysis of aqueous environments employed for supporting photo-ALE of GaAs/$Al_{0.35}Ga_{0.65}As$ nanoheterostructures. The ICP-MS technique is capable of providing a highly precise and quantitative determination of elements owing to the invention of chromatographic detectors.[37] A dilution of analyzed liquid samples in HNO_3 and deionized (DI) water allows for the separation of matrix elements, which is important in view of the high volatilities of both Ga and As chlorides.[38] A comparison between the ICP-MS detected ions and those released by the photoetching nanoheterostructure of a well-defined thickness made possible the investigation of the conditions for the formation of stoichiometric surfaces. A correlation between ICP-MS and PL data concerning constant photo-ALE rates indicated the feasibility of this approach for the attractive in situ monitoring of the formation of stoichiometric or near-stoichiometric surfaces of interest to nanostructuring and in situ passivation of III−V semiconductor nanodevices.

2. EXPERIMENTAL SECTION

2.1. GaAs/AlGaAs Nanoheterostructures. The GaAs/$Al_{0.35}Ga_{0.65}As$ wafer J0152 was grown by molecular beam epitaxy (CPFC, National Research Council of Canada, Ottawa) on a semi-insulating GaAs (001) substrate. It consists of a 20-pair AlAs/GaAs (2.4 nm/2.4 nm) superlattice applied as a barrier against the propagation of defects and a 500 nm thick GaAs PL emitter. A 100 nm thick $Al_{0.35}Ga_{0.65}As$ layer, a 3 nm thick GaAs layer, and a 10 nm thick $Al_{0.35}Ga_{0.65}As$ layer were grown on the top of the GaAs emitter. The nanoheterostructure was capped with an 8 nm thick GaAs layer. The D3422 wafer was also grown by metal organic chemical vapor deposition (CPFC, National Research Council of Canada, Ottawa) on a semi-insulating GaAs (001) substrate. This consists of a 20-pair AlAs/GaAs (2.4 nm/2.4 nm) superlattice and a 500 nm GaAs layer, followed by a 100 nm thick $Al_{0.35}Ga_{0.65}As$ layer. However, in this case, six pairs of 12 nm thick GaAs and 10 nm thick $Al_{0.35}Ga_{0.65}As$ were grown and capped with a 12 nm thick GaAs layer.

Figure 1 shows a cross section of GaAs/AlGaAs nanoheterostructures employed in this work, along with their room-temperature PL spectra obtained with a commercial Philips PL mapper (PLM-150). The nanoheterostructures were excited with a second harmonic of Nd:YAG laser source (λ_{ex} = 532 nm), and the emitted PL signal was collected with an InGaAs photodiode detector array. The PL mapping spatial and spectral resolutions were 20 μm and 0.6 nm, respectively. Both wafers shown in Figure 1 emitted PL with the

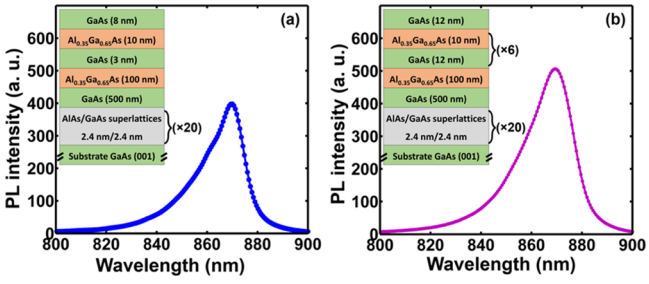

Figure 1. Room-temperature PL spectra of GaAs/$Al_{0.35}Ga_{0.65}As$ nanoheterostructures taken from J0152 wafer (a) and D3422 wafer (b). Samples were excited with a 532 nm laser beam of the Philips PL mapper (PLM-150). In both cases, the PL emission originated from 500 nm thick GaAs layers shown in cross section of the investigated samples.

DOI: 10.1021/acsami.9b02079
ACS Appl. Mater. Interfaces 2019, 11, 17968−17978

maximum at $\lambda \approx 870$ nm originating from the 500 nm thick GaAs epitaxial layer. No PL emission was observed at room temperature from other GaAs layers sandwiched between AlGaAs barriers or from the AlAs/GaAs superlattice. At 20 K, a quantum confined PL peak at 724 nm was observed from the 3 nm thick GaAs layer of the J0152 wafer. The intensity of that peak was found at ~6 times weaker than that of the bulk GaAs at 821 nm (see Figure S1).

2.2. Photo-ALE Process of GaAs/AlGaAs Nanoheterostructures. Individual samples were mounted in a Teflon holder capped with an optically transparent window and irradiated intermittently for 3 s in each 60 s cycle [duty cycle (DC) = 3/60] or for 3 s in each 25 s cycle (DC = 3/25). This made it possible to observe the photoetching at relatively low rates. Figure 2 displays a schematic view of the photo-

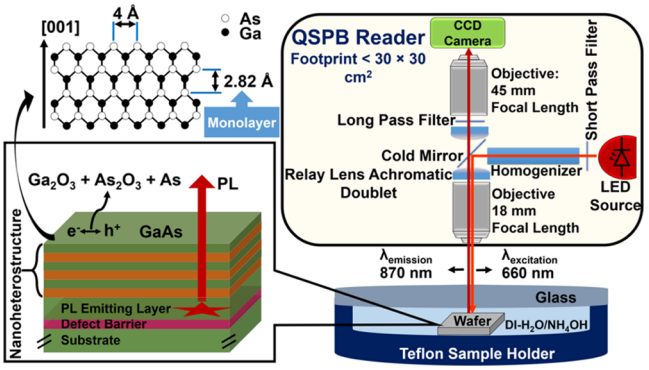

Figure 2. Schematic view of the setup employed for photo-ALE of $GaAs/Al_{0.35}Ga_{0.65}As$ nanoheterostructures. Samples were irradiated with λ = 660 nm of LED. PL emission from a 500 nm thick GaAs layer was recorded using a CCD camera.

ALE setup employed for the processing of GaAs/AlGaAs nanoheterostructures. The measurements of PL emission were carried out with a custom-made quantum semiconductor photonic biosensing reader described elsewhere.[31] Briefly, a homogenized beam of a 660 nm light-emitting diode (LED) allowed for simultaneous excitation of the entire surface of a sample. The PL emission of the GaAs/$Al_{0.35}Ga_{0.65}As$ nanoheterostructures was filtered in the range of 840–1650 nm (long pass filter, Edmunds 86-070), and the spatially resolvable intensity maps were collected with a CCD camera. A calibrated Si photodiode (S130C, Thorlabs, NJ, USA) was employed to monitor the LED power (P) during the photo-ALE experiments. The cycled irradiation of samples, with a nonirradiation period designed to give enough time for the photocorrosion products to dissipate into the etching environment of DI H_2O or NH_4OH, allowed us to observe etch rates below 2.82 Å/cycle, that is, corresponding to the thickness of a monolayer of GaAs.

2.3. Sample Preparation. Samples of 2 mm by 2 mm size were cut out from photoresist (S1813, Shipley)-coated wafers. Following the exposure to acetone for 5 min and ultrasonication (designed to remove the photoresist), the samples were degreased in an ultrasonic bath of OptiClear, acetone, and isopropyl alcohol (IPA) each for 5 min. Samples were dried with high-purity nitrogen 4.8 HP (99.998%). Then, they were exposed to an aqueous solution of ammonium hydroxide (NH_4OH at 28%) for 2 min and rinsed with DI H_2O.

2.4. Chemicals. Chemicals were purchased from the following sources: OptiClear from National Diagnostics (Mississauga, Canada), acetone from ACP (Montréal, Canada), IPA from Fisher Scientific (Ottawa, Canada), ammonium hydroxide 28% (NH_4OH) from Anachemia (Richmond, Canada), and high-purity nitrogen 4.8 HP (99.998%) from Praxair Canada Inc. (Mississauga, Canada). The 18.2 MΩ DI H_2O, used in these experiments, was produced by means of a customized Millipore purification system assembled by Culligan (Quebec, Canada).

2.5. Inductively Coupled Plasma Mass Spectrometry. The solutions containing photo-ALE products were collected for ICP-MS analysis at the end of each photo-ALE experiment in DI H_2O or NH_4OH. To adjust the results for dark corrosion, witness samples were immersed in DI H_2O or NH_4OH and kept in darkness for the same period of time as the photoetching samples. The ICP-MS experiments were carried out in a PerkinElmer ELAN DRC II ICP-MS equipped with an AS-93 auto sampler. Data were collected for 5 mL samples with 20 sweeps per reading, 1 reading per replicate, and 3 replicates for each sample. The dwell time was 50 ms/AMU. Germanium was used as an internal standard. Both the internal standard and the sample were introduced into the machine via a peristaltic pump and mixed in a T junction just before entering the nebulizer. The injection sequence was a 45 s wash with 2% nitric acid, followed by a 75 s flush with the sample. A 15 s delay was applied before taking a reading. The standard curve for calculation was prepared from 1000 ppm ICP-MS grade single element standard (Isospec, Delta Scientific) and 2% nitric acid as the diluting solvent. Calibration was carried out for the 1–500 ppb range. The diluting solvent and wash solutions were prepared from Aristar plus nitric acid (BDH ARISTAR) and ultrapure water (18.2 MΩ/cm, ELGA purifying machine). Samples were kept at room temperature between reception and ICP-MS analysis.

2.6. Fourier Transform Infrared Spectroscopy. Analysis of the surface chemistry of photoetched samples was carried out based on the Fourier transform infrared spectroscopy (FTIR) absorption data collected with a Vortex 70v instrument (FTIR Bruker, Germany). Typically, an absorption spectrum was constructed based on 512 scans collected with a mercury cadmium telluride (MCT) detector. Measurements started with a 15 min delay after evacuation of the sample compartment to minimize the influence of moisture on the collected data. A freshly prepared (degreased, then immersed for 2 min in NH_4OH, rinsed with DI H_2O, and dried with nitrogen flow) J0152 GaAs/AlGaAs sample was used to determine an FTIR absorption baseline. FTIR data were analyzed to resolve absorption peaks using OPUS software (version 7.2).

2.7. Atomic Force Microscopy. The surface morphology of processed samples was studied using an atomic force microscopy (AFM) technique (Digital Instrument, Nanoscope III). The AFM instrument was operated in a tapping mode. All images were collected over a 10 μm × 10 μm surface area with 512 points per line for 512 lines, using a tip velocity of 12 μm/s and at a scan rate of 0.598 Hz. A freshly prepared (degreased, then immersed for 2 min in NH_4OH, rinsed with DI H_2O, and dried with nitrogen flow) J0152 GaAs/AlGaAs sample was used as the reference surface.

2.8. X-ray Photoelectron Spectroscopy. The X-ray photoelectron spectroscopy (XPS) Kratos Axis Ultra DLD spectrometer was utilized to determine the elemental composition of the sample surface. Samples were excited with the Al Kα monochromatized line (1486.6 eV) of a 225 W source. The analyzer was operated in a constant pass energy mode of 160 eV for the survey scans and 20 eV for the high-resolution scans. The work function of the instrument was calibrated to give a binding energy (BE) of 83.96 eV for the Au $4f_{7/2}$ line of metallic gold. The dispersion of the spectrometer was adjusted to give a BE of 93.62 eV for the Cu $2p_{3/2}$ line of metallic copper. The samples were mounted on a nonconductive tape. A charge neutralizer was used on all samples to compensate for the charging effect. Charge corrections were done using the adventitious carbon peak set at 284.8 eV. The analyzed area was an oval with approximate dimensions of 300 μm × 700 μm. Data analysis was conducted using CasaXPS software (version 2.3.18). The relative sensitivity factors used for quantification purposes are the experimental RSF given by Kratos Analytical for their machines.

3. RESULTS

Figure 3 shows examples of the integrated temporal PL intensity from four individual samples of the J0152 wafer that underwent photo-ALE in DI H_2O following 90, 266, 450, and 720 cycle numbers (CNs) for DC (DC = T_{ON}/T_{TOT}) equal to 3/60 and P = 20 mW/cm^2. The formation of well-defined PL maxima could be clearly observed in agreement with the previously reported results.[31,32,35,36] This figure illustrates the

DOI: 10.1021/acsami.9b02079
ACS Appl. Mater. Interfaces 2019, 11, 17968–17978

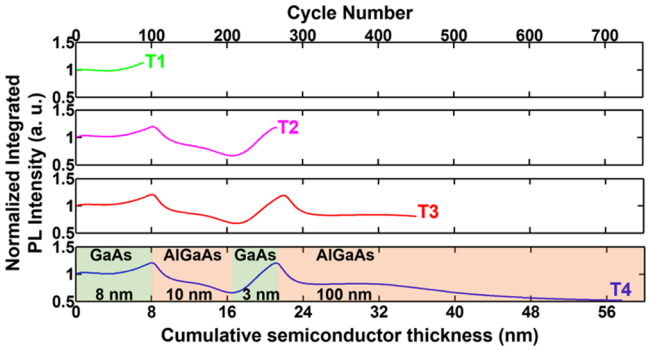

Figure 3. Temporal GaAs PL emission from four J0152 samples that underwent photo-ALE in DI H_2O as a function of the semiconductor thickness (CN) for DC = 3/60. The zones of etched GaAs and AlGaAs layers are indicated approximately with distinctively different colors.

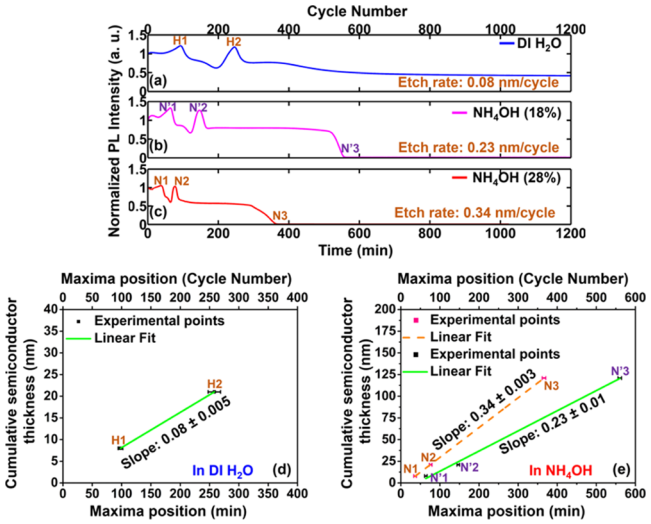

Figure 4. Representative temporal PL intensities of J0152 samples that underwent photo-ALE in DI H_2O (a), 18% solution of NH_4OH (b), and 28% solution of NH_4OH (c). The cumulative thickness of the nanoheterostructure that underwent photo-ALE in DI H_2O vs positions of the first and second PL maxima (d). The cumulative thickness of the nanoheterostructure that underwent photo-ALE in 18 and 28% NH_4OH solutions vs positions of the first and second PL maxima and the last AlGaAs/GaAs interface (e).

important reproducibility of the photo-ALE process (see also Figure S1b). As a guide to an eye, the zones of photoetching GaAs and $Al_{0.35}Ga_{0.65}As$ layers extending up to 56 nm, that is, deep inside of the 100 nm thick $Al_{0.35}Ga_{0.65}As$ layer, were indicated in this figure. The initial increase of the PL signal, observed in Figure 3 for CN ≤ 100, is related mainly to the formation of Ga_2O_3 that is known to reduce the concentration of nonradiative recombination centers (NRRCs) and chemically passivate the GaAs surface.[39] As the GaAs layer was dissolved, the formation of an electrolytic junction involving DI H_2O and $Al_{0.35}Ga_{0.65}As$ revealed an interface with a significantly greater surface concentration of NRRCs. A reduced intensity of the PL emission, each time the $Al_{0.35}Ga_{0.65}As$ surface is exposed to DI H_2O, is consistent with the greater surface recombination velocity of AlGaAs (~10^7 cm/s) in comparison to that of 10^5 to 10^6 cm/s observed for the GaAs surface.[40,41] The PL signal begins to recover only when a new electrolytic junction involving DI H_2O and GaAs is formed in situ (observed for CN > 210). Consequently, temporal positions of the PL maxima can be accurately correlated with the position of GaAs/AlGaAs interfaces, consistent with the AFM-measured depth of photocorroded craters in GaAs/AlGaAs quantum well microstructures.[35] Furthermore, positions of PL maxima versus time are directly related to the rate of material removal, which can be controlled by the power and sequence (DC) of the excitation photons[35] as well as the pH of surrounding solution.[32]

Figure 4 displays temporal PL of J0152 samples photoetched at different rates in DI H_2O and aqueous solutions of NH_4OH. As can be seen in Figure 4a, after ~600 cycles, the PL intensity of the sample photoetched in DI H_2O was found to stabilize at ~ 50% of the initial intensity. However, photoetching in NH_4OH, with ~ less than 600 cycles (Figure 4b) and less than 400 cycles (Figure 4c), resulted in PL signals that are too weak to be detected with the employed PL setup and relatively weak excitation conditions (P = 20 mW/cm^2). Figure 4d,e shows examples of temporal PL intensity plots for J0152 samples that underwent photo-ALE in DI H_2O and NH_4OH solutions. On the basis of the estimated positions of the PL-revealed GaAs/AlGaAs interfaces, the initial etch rate of this material in DI H_2O was at 0.08 ± 0.005 nm/cycle, that is, approximately 0.3 monolayer/cycle.[42] However, the photocorrosion in this environment is not sustainable because of the surface accumulation of the poorly dissolvable oxides. This is manifested by the constant intensity of a PL signal observed for CN > 600 in Figure 4a. In contrast, the processes carried out in both 18 and 28% aqueous solutions of NH_4OH (see also Figure 7b) are illustrated by the vanishing PL signals as the etching front reaches the surface of a 500 nm thick GaAs PL emitter (N3 and N′3). These data illustrate the attractive potential of employing the PL effect to study the congruently decomposing III−V materials.

To further investigate the underlying mechanisms responsible for conditions leading to the congruent decomposition of the investigated nanoheterostructures and, ultimately, to the formation of stoichiometric surfaces, the analysis of photo-ALE products was carried out with ICP-MS measurements. The number of As^{3+} and Ga^{3+} ions expected to be released by photo-ALE GaAs/$Al_{0.35}Ga_{0.65}As$ nanoheterostructures of known thicknesses was compared to those determined by ICP-MS. The calculations of released As^{3+} and Ga^{3+} ions were based on the empirically determined etch rates, shown in Figure 4d,e, as well as on the known thickness of GaAs/$Al_{0.35}Ga_{0.65}As$ nanoheterostructures (see the Supporting Information for details). A comparison between ICP-MS detected As^{3+} and Ga^{3+} ions with the calculated ion concentrations expected to be released during photo-ALE of the GaAs/$Al_{0.35}Ga_{0.65}As$ nanoheterostructures in DI H_2O and NH_4OH is shown in Figure 5. Notice that different concentrations of ions calculated in DI H_2O and NH_4OH for the same amount of the photoetched material are due to the different molecular weights of the investigated solutions. It can be seen that ICP-MS detected As^{3+} and Ga^{3+} ions at 110 and 18 ppb, respectively, were released from the nanoheterostructure photoetched by 60 nm in DI H_2O. These results were adjusted for the dark corrosion that revealed up to ~20 and ~5 ppb of As^{3+} and Ga^{3+} ions, respectively, released during the same period of time (see Figure S2). While a growing deficit of As^{3+} ions was detected for the samples photoetched deeper than 60 nm (Figure 5a), a deficit of Ga^{3+}

DOI: 10.1021/acsami.9b02079
ACS Appl. Mater. Interfaces 2019, 11, 17968−17978

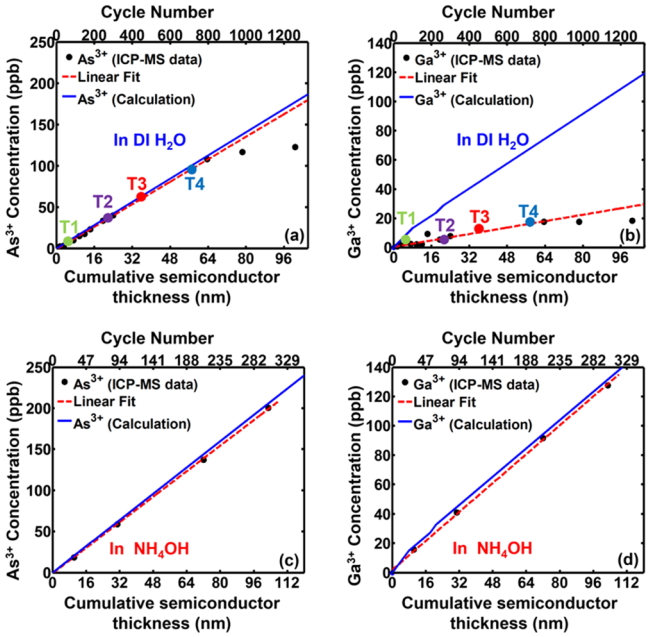

Figure 5. Comparison of ICP-MS detected As^{3+} and Ga^{3+} ions with their calculated concentrations expected to be released during photo-ALE of GaAs/$Al_{0.35}Ga_{0.65}As$ nanoheterostructures in DI H_2O (a,b) and NH_4OH (c,d), respectively. Data collected at the end of runs T1−T4 that were previously shown in Figure 3 are indicated with large full circles in Figure 5a,b.

ions could already be observed for a sample photoetched by less than 8 nm (Figure 5b). This is consistent with the inability to induce congruent decomposition of GaAs in DI H_2O. In contrast, the ICP-MS detected concentrations of both As^{3+} and Ga^{3+} ions were in excellent agreement with the calculated data for the nanoheterostructure that underwent photo-ALE in NH_4OH by at least ∼110 nm (Figure 5c,d).

The photo-ALE process of III−V semiconductors is based on the presence of holes required for chemical modification (oxidation) and decomposition, with the main products of GaAs photoetched in water being $[Ga(OH)_4]^-$, GaO, Ga_2O, Ga_2O_3, and AsO.[43,44] The oxidation/decomposition process of GaAs in water is described by the following reaction[45]

$$2GaAs + 3h^+ + 3H_2O \rightarrow Ga_2O_3 + 2As(0) + 6H^+ \quad (1)$$

where h^+ represents the hole carriers. Following the absorption of e−h^+-forming photons, Ga^{3+} ions produced at the GaAs surface could react with dissolved oxygen or oxygen of water molecules and produce Ga oxides. Among As oxides and Ga oxides, Ga_2O_3 represents a relatively stable form of a compound that is insoluble in water, and thus, it could accumulate at the GaAs surface.[46] Furthermore, some of the Ga^{3+} ions could diffuse out from the surface and form oxides in the solution. Ultimately, the contribution of these two processes leads to the presence of Ga^{3+} ions in the aqueous environment. Photo-oxidation of GaAs also produces As oxides. The elemental As(0) formed at the surface in the first step (reaction 1) could react further, giving As_2O_3 as the main product of the following reaction[47]

$$2As(0) + 3h^+ + 3H_2O \rightarrow As_2O_3 + 6H^+ \quad (2)$$

Thus, As_2O_3 could also be formed in the solution. However, this compound is both volatile and water-soluble under neutral pH conditions.[47] This leads to the decomposition of GaAs into Ga_2O_3 and the formation of elemental As, as follows[48]

$$2GaAs + As_2O_3 \rightarrow Ga_2O_3 + 4As \quad (3)$$

The reaction 3 which is kinetically slow but thermodynamically favored[46] could increase the concentration of As in a solution. Considering these reactions, Ga products in DI H_2O are expected to partially remain on the surface of III−V samples. However, the accumulation of such oxides in NH_4OH is prevented.[49] The characterizations of J0152 samples with FTIR, XPS, and AFM techniques made it possible to further clarify the process of photo-ALE of GaAs and $Al_{0.35}Ga_{0.65}As$ in DI H_2O and NH_4OH.

Figure 6 compares high-resolution XPS scans of four J0152 samples that underwent photo-ALE with the XPS scan for a freshly prepared reference sample partially covered with native

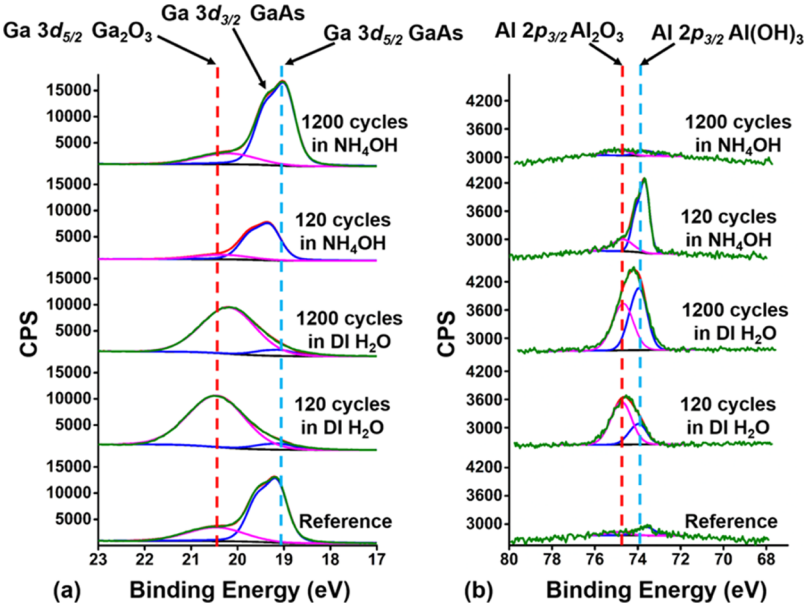

Figure 6. High-resolution XPS scans for Ga 3d (a) and Al 2p (b) transitions in J0152 samples that underwent photo-ALE in DI H_2O and NH_4OH.

DOI: 10.1021/acsami.9b02079
ACS Appl. Mater. Interfaces 2019, 11, 17968−17978

oxide (following etching in NH_4OH, that sample was air-exposed for ~30 min before being loaded into the XPS chamber). Figure 6a shows two peaks related to the Ga 3d transitions differentiated by a chemical shift. The peaks in the higher energy region of BE equal to 20.2 eV[50] and 20.5 eV[51] contribute to the integrated peak corresponding to an oxide state of GaAs. The energy peak at BE = 19.28 eV[52] corresponds to Ga bound in GaAs. In the case of samples photoetched in H_2O, the Ga_2O_3 peak (BE = 20.5 eV) was always present, and its intensity was much higher than that of the native oxide of the reference sample. In contrast, the intensity of this peak for the samples that underwent photo-ALE in a NH_4OH environment was fairly similar to that of the reference sample. This is consistent with the dissolution and/or growth prevention of Ga oxide in the NH_4OH environment. High-resolution scans of Al 2p, displayed in Figure 6b, indicated two types of aluminum compounds, Al_2O_3 with BE = 74.7 eV[53] and $Al(OH)_3$ with BE = 73.9 eV,[54] formed at the surface of the investigated samples as a result of Al reacting with H_2O and Al with O_2. Because of the small difference between BEs corresponding to these compounds, they are known to be difficult to differentiate.[55] In the case of the $GaAs/Al_{0.35}Ga_{0.65}As$ nanoheterostructure that underwent photo-ALE with 120 CN in NH_4OH (~36 nm deep according to Figure 4e), the XPS probed surface was mostly that of $Al_{0.35}Ga_{0.65}As$, and the corresponding amount of $Al(OH)_3$ was much higher than that of Al_2O_3. This suggested that accumulation of Al_2O_3 was slightly inhibited in the NH_4OH environment. Of particular importance to the constant etch rate is that the XPS Al $2p_{3/2}$ scan, as shown in Figure 6b, revealed neither Al_2O_3 nor $Al(OH)_3$ related peaks for the sample that underwent photo-ALE with 1200 CN, that is, up to ~411 nm deep (based on the average photo-ALE rate of 0.34 nm/cycle, as shown in Figure 4e). This suggests that a CN proportional concentration of Al ions should be expected in a photo-ALE product generated in the NH_4OH environment. However, such an agreement could not be demonstrated, probably because of the poor sensitivity of the ICP-MS method to Al ions in this experiment. A possible reason for this difficulty could also be the relatively high vapor pressure of NH_4OH, which is known to be the source of the ICP instability.[56] Alternatively, NH_4OH could induce precipitation of Al as an insoluble hydroxide.[57]

Figure 7 compares PL plots collected during photo-ALE of the D3422 wafer consisting of seven pairs of 12 nm thick GaAs and 10 nm thick $Al_{0.35}Ga_{0.65}As$ layers. These experiments were carried out with LED power $P \approx 16$ mW/cm^2 and DC = 3/25. One can see that it took ~1920 CN to reveal seven PL maxima of this nanoheterostructure processed in DI H_2O (Figure 7a), while only 725 CN revealed the same number of peaks in NH_4OH (Figure 7b). Furthermore, photo-ALE in the oxide etching environment of NH_4OH[22,49] made it possible to define the positions of each PL maximum more precisely than in the DI H_2O environment. Figure 7c shows that the positions of the PL maxima detected in NH_4OH follow a straight line as a function of the cumulative thickness of the nanoheterostructure that underwent photo-ALE to at least 80 nm deep, which is consistent with the constant etch rate. In contrast, a growing deviation from such a linear behavior was already observed for the similar nanoheterostructure that underwent photo-ALE in DI H_2O to less than 40 nm. Thus, these results indicate that the process of a congruent decomposition of $GaAs/Al_{0.35}Ga_{0.65}As$ nanoheterostructures could be monitored conveniently with the PL effect.

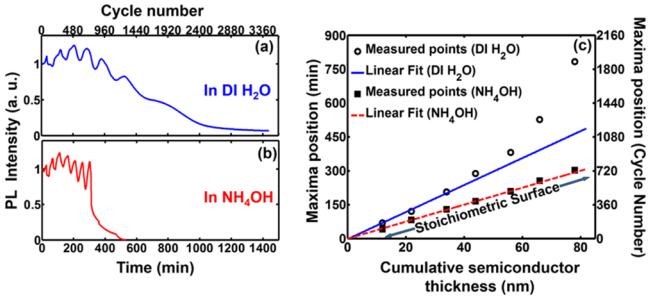

Figure 7. Photo-ALE of GaAs/AlGaAs nanoheterostructures (wafer D3422). Temporal PL plots from the samples processed in DI H_2O (a) and NH_4OH (b). Linearly dependent PL maxima positions on the cumulative thickness of the $GaAs/Al_{0.35}Ga_{0.65}As$ nanoheterostructure indicate a congruent decomposition process (c).

Figure 8 shows AFM images of a J0152 reference sample (Figure 8a), S1−S4 samples after photo-ALE in DI H_2O with 40, 120, 180, and 322 CN (Figures 8b−8e), and an S5 sample after photo-ALE in NH_4OH with 322 CN (Figure 8f). 3D AFM images of these samples have also been included in the Supporting Information (Figure S5). It can be seen that the surface morphology of the samples that underwent photo-ALE in DI H_2O up to a depth of ~14.4 nm (S1−S3) is characterized by σ_{RMS} = 0.76−0.86 nm, which is fairly comparable to σ_{RMS} = 0.75 nm which characterizes the reference sample. However, the sample S4, which underwent photo-ALE to a depth of ~105.6 nm in DI H_2O, is characterized by σ_{RMS} = 2.1 nm (Figure 8e). The increased roughness of that sample is likely related to the surface precipitation of Ga_2O_3 and, consistent with the XPS results (Figure 6a), to the presence of some Al compounds insolvable in DI H_2O. In contrast, the surface of the S5 sample that underwent photo-ALE in NH_4OH to a comparable depth of ~105.6 nm (Figure 8f) is characterized by σ_{RMS} = 0.93 nm, which is minimally greater than σ_{RMS} = 0.75 nm of the reference sample (Figure 8a).

4. DISCUSSION

Conventional ALE allows monolayer or submonolayer precision of material removal based on the formation, through a self-terminated reaction, of an altered layer of the material at the surface of a processed material. The concept of a photo-ALE technique discussed in this report is based on the formation of an altered layer of the processed material involving photoexcited holes (see reaction 1). Normally, this process is carried out in a liquid solution designed to dissolve the altered layer.

The efficiency of generating a PL signal by a semiconductor is related to the minority carriers lifetime, τ, and it could be expressed with the following relationship[58]

$$\frac{1}{\tau} = \frac{1}{\tau_R} + \frac{1}{\tau_{nR}} + \frac{IRV}{d} \quad (4)$$

where τ_R and τ_{nR} denote the lifetime of radiative and nonradiative recombination processes, respectively, d is the thickness of the active (PL emitting) layer, and IRV (interface recombination velocity) represents processes related to the interface states of the investigated materials. In the case of the GaAs and $Al_{0.35}Ga_{0.65}As$ nanoheterostructures investigated in

DOI: 10.1021/acsami.9b02079
ACS Appl. Mater. Interfaces 2019, 11, 17968−17978

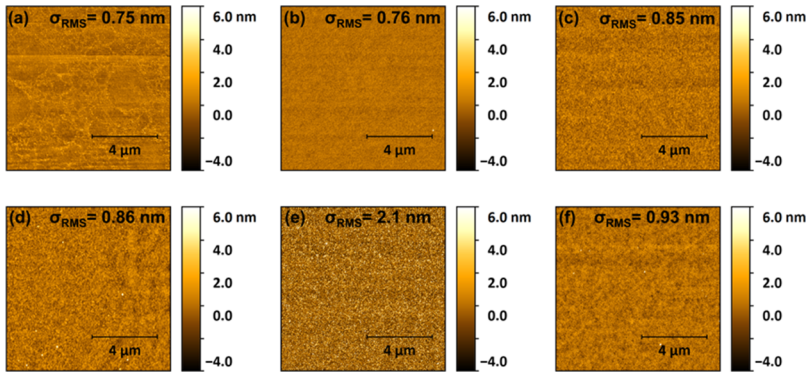

Figure 8. AFM images of J0152 samples taken for a freshly prepared reference sample (a), after photo-ALE in DI H_2O to depths of 3.2 (b), ∼9.6 (c), ∼14.4 (d), ∼105.6 nm (e), and after photo-ALE in NH_4OH to a depth of ∼105.6 nm (f).

this report, the overall IRV is a sum of the recombination velocities, IRV_k, at interfaces of the PL-emitting GaAs layer with $Al_{0.35}Ga_{0.65}As$ and AlAs, at interfaces between GaAs and $Al_{0.35}Ga_{0.65}As$ layers located above, as well as at the interface of the topmost layer with the etching solution, that is, IRV = $\sum_{k=1}^{n} IRV_k$. In addition to the presence of the intrinsic surface states arising from the break in the translational symmetry of a bulk semiconductor at its surface, the impurities and other surface defects act as NRRC playing a critical role in the conversion efficiency of excited electron−hole pairs to the PL signal. Therefore, the oscillation of PL intensity of the GaAs/AlGaAs nanoheterostructures is related to the variations of the surface states as a result of the formation/dissolution of surface oxides. For instance, the two PL maxima in Figure 3 observed at ∼110 CN and ∼270 CN are related to the onset of the formation of AlGaAs−H_2O interfaces.

The ICP-MS data made it possible to determine the conditions, leading to the congruent decomposition of the investigated nanoheterostructures. A colinear dependence between calculated and ICP-MS detected As^{3+} ions, as observed in Figure 5a for samples photoetched up to 60 nm deep in DI H_2O, suggests the presence of such an effect. However, a deficit of Ga^{3+} ions in the photo-ALE product observed from the early stage of the process (Figure 5b) indicates that it is impossible to induce a congruent decomposition of GaAs and AlGaAs in DI H_2O. In contrast, photo-ALE in 28% of NH_4OH presented in Figure 5c,d demonstrated an excellent agreement between the concentrations of As^{3+} and Ga^{3+} ions detected in the photo-ALE product and those expected for these ions released by the photoetching nanoheterostructures, at least up to ∼110 nm deep. The congruent character of the observed decomposition is consistent with the formation of stoichiometric surfaces of GaAs and AlGaAs at the end of each etching cycle.

The photo-ALE process is based on a negligible dark corrosion in the processing environment. For GaAs, even in a heavily oxidizing environment of H_2O_2, the thickness of the surface oxide saturates at ∼10 nm after a 6-day exposure at room temperature.[22] The absence of a significant dark corrosion in H_2O has also been confirmed by our ICP-MS data (Figure S3), revealing that the number of ions released in darkness after ∼22 h is comparable to the amount of a GaAs/AlGaAs nanoheterostructure photocorroded during an accumulated light exposure of less than 10 min (16 nm thick GaAs/AlGaAs nanoheterostructure). During light-on phase with the above band gap photons of GaAs surrounded by the water environment, the photoholes created by the absorbed photons induce the oxidation process described by reactions 1−3. Because it is possible to abruptly terminate the flux of photoholes by switching off the irradiation source, this method makes etching precision possible at the submonolayer level. The formation of Ga_2O_3 along with other surface oxides and $Al(OH)_3$ has been observed during the light-on phase (see Figures 6 and S4). The presence of Ga_2O_3 on the GaAs surface reduces the number of surface NRRCs, which is manifested by the enhanced GaAs PL. We have explored this effect for detecting electrically charged biomolecules perturbing the surface states of GaAs (see, e.g., ref 31). Although Ga_2O_3 is relatively stable in water environment,[59] other surface photoproducts undergo a slow dissolution that, depending on the pH of an aqueous solution, could lead to their accumulation.[32] Clearly, while the duration of a light-on phase determines the surface coverage with Ga_2O_3 and other oxides, the light-off phase is designed to entirely dissolve the surface accumulating photocorrosion products. In this work, we employed an aqueous solution of NH_4OH for this purpose. Empirically, we found that a 3 s irradiation with 20 mW/cm^2 covers the GaAs surface with photoproducts that dissolve entirely within 57 s if the process is carried out in an aqueous solution of at least 18% NH_4OH (see Figure 4b,c). Note that this step is self-limiting as long as the dark corrosion is negligible. In contrast, the same process in DI H_2O leads to the accumulation of surface oxides, manifested by the vanishing photocorrosion as suggested by the constant intensity of a PL signal observed for CN > 500 in Figure 4a. Thus, while the true photo-ALE of GaAs in H_2O could take place only during the initial phase (few cycles) of the process, the exact photo-ALE of GaAs takes place in an NH_4OH environment (see Figure 4b,c). It is expected that depending on the III−V microstructure of interest, different chemistry as well as process parameters, such as the excitation power, DC, time-off, temperature, and so forth, will have to be investigated.

The interaction of Al ions, released by photoetching of AlGaAs, with H_2O and O_2 could lead to the formation of Al_2O_3 and $Al(OH)_3$.[55] Indeed, the Al−O stretching mode (520 cm^{-1}) identified with the FTIR data shown in Figure S4 points out to the presence of Al_2O_3. Consistent with this are the high-resolution XPS scans for Ga 3d and Al 2p shown in Figure 6 that confirm the presence of Ga_2O_3 as well as Al_2O_3 and $Al(OH)_3$. These compounds could prevent diffusion of O or H_2O molecules toward the oxide−semiconductor interface, resulting in reduced photoetching rates. However, no Al ions were detected in the photo-ALE product with the ICP-MS measurements. The absence of Al ions in the ICP-MS data of

DOI: 10.1021/acsami.9b02079
ACS Appl. Mater. Interfaces 2019, 11, 17968−17978

photo-ALE samples could imply that Al compounds, due to their poor solubility in NH_4OH[49,60] and water,[60] remained on the surface of photoetching samples. Alternatively, the inability to detect Al ions in NH_4OH could be related to the known difficulty of the ICP-MS technique in tracing metals in NH_4OH.[56,57]

The unique ability of the photo-ALE process to provide a rapid assessment of the semiconductor etching characteristics was further underscored by photo-ALE data of wafers with multiple nanoheterostructures (Figure 7). Under constant photo-ALE rates, the positions of PL-revealed maxima (interfaces) depend linearly on the thickness of the investigated nanoheterostructures. This was achieved for a D3433 sample etched in NH_4OH up to 80 nm deep, as presented in Figure 7b (full squares). The use of NH_4OH for deep photo-ALE of AlGaAs nanoheterostructures must be further explained as it is known that NH_4OH-based solutions were used for selective etching of GaAs over AlGaAs.[49−61] This is because the Al−O bond is much stronger than that of Ga−O and As−O, which would lead to surface accumulation of Al_2O_3. Thus, it is plausible to expect that the linear (CN proportional) etching of the GaAs/AlGaAs nanoheterostructures investigated here, significantly thicker than 80 nm, would require Al-oxide etching solutions, such as hydrofluoric acid or phosphoric acid.[49] In contrast, PL data for the same nanoheterostructures photoetching in DI H_2O (Figure 7c, open circles) suggest that nonlinear photoetching takes place at depths exceeding 35 nm. This is consistent with the decelerating photo-ALE rate because of accretion of Ga_2O_3 (Figure 7a) and with the significant deficit of Ga^{3+} ions detected with ICP-MS, for more than ∼8 nm of etched GaAs (Figure 5b). It appears that a more accurate PL-based assessment of the photo-ALE process would still be possible, for example, by reducing the average amount of material etched in an individual photo-ALE cycle.

The AFM data revealed that the surface of the GaAs/AlGaAs nanoheterostructure photoetched in NH_4OH was smoother (Figure 8f, σ_{RMS} = 0.93 nm) compared to the surface of that nanoheterostructure photoetched in DI H_2O to a comparable depth (Figure 8e, σ_{RMS} = 2.1 nm). Furthermore, the photo-ALE process of J0152 etched in DI H_2O to less than ∼14 nm (Figure 8b−d) did not significantly increase the surface roughness of the processed samples. Hence, consistent with the XPS and FTIR data, the source of the increased roughness must be related to the surface accumulated oxides poorly dissolvable in DI H_2O. Clearly, while etching in NH_4OH eliminates the accumulation of Ga and As oxides on the etched surfaces, the use of ammonia is not efficient in removing Al oxides and Al-based compounds. As the accumulation of these products is expected in proportion to the overall thickness of photo-ALE GaAs/AlGaAs nanoheterostructures, it is reasonable to expect that the presence of these products is responsible for the increased surface roughness of the 105.6 nm deep etched sample (σ_{RMS} = 0.93 nm). Nevertheless, the σ_{RMS} values reported here require additional discussion as it is known that high-quality GaAs (001) surfaces are characterized by $\sigma_{RMS} \leq 0.5$ nm (e.g., Karkare and Bazarov[62]), and chemo-mechanical polished (CMP) epi-ready GaAs (001) could have $\sigma_{RMS} \leq 0.15$ nm.[63] Notice that the samples investigated in this report were diced out from a wafer that was photoresist-coated to minimize the inclusion of semiconductor dust generated during dicing. This procedure was carried out in a fabrication environment class 10000, and no special surface treatment, such as CMP or thermal annealing, was applied to these samples after photoresist removal. Under these conditions, σ_{RMS} = 0.75 nm for the reference sample (Figure 8a) seems a reasonable result.

5. CONCLUSIONS

We investigated the mechanisms of photo-ALE of GaAs/$Al_{0.35}Ga_{0.65}As$ nanoheterostructures in DI H_2O and NH_4OH environments. The photocorroding was induced with a low power 660 nm LED ($P \approx 16-20$ mW/cm^2) and monitored in situ with PL emitted by the investigated nanoheterostructures. The ICP-MS detected concentrations of the photo-ALE products were compared to the calculated concentrations of As^{3+} and Ga^{3+} ions expected to be released by photocorroded GaAs and AlGaAs layers of known thickness. A deficit of Ga^{3+} ions in the photo-ALE product was detected for the nanoheterostructures photocorroded in DI H_2O, suggesting that it is impossible to produce stoichiometric surfaces of GaAs or AlGaAs dissolving in such an environment. In contrast, the ICP-MS results exhibited an attractive agreement between the concentrations of As^{3+} and Ga^{3+} ions in the photo-ALE products and those expected for As^{3+} and Ga^{3+} ions released by the nanoheterostructures photocorroded in NH_4OH, at least up to ∼110 nm deep. The congruent character of the decomposition in this case was consistent with the constant photo-ALE rate and formation of stoichiometric surfaces. The constant photo-ALE rate of GaAs was also demonstrated with PL data for the nanoheterostructures photocorroded in NH_4OH. The AFM data confirmed the formation of a relatively smooth surface (σ_{RMS} = 0.93 nm) of a GaAs/AlGaAs nanoheterostructure (J0152) photocorroded in NH_4OH to a depth of 105.6 nm. In contrast, the surface of that nanoheterostructure photocorroded to a comparable depth in DI H_2O was significantly rougher (σ_{RMS} = 2.1 nm), consistent with the surface accumulation of Ga_2O_3 and other Al-based compounds. Because $Al(OH)_3$ and Al_2O_3 could pile up on the surface of GaAs/AlGaAs nanoheterostructures photocorroded in NH_4OH, the fabrication of the stoichiometric surface of nanoheterostructures photocorroded significantly deeper than100 nm requires Al compound etching environments, such as those comprising hydrofluoric or phosphoric acids.

The concept of photo-ALE is similar to the conventional ALE of silicon, metals, and some oxides. However, there are some fundamental differences pointing to the potential advantage of a photoprocess in the nanostructuring of compound semiconductors and fabrication of advanced nanoscale devices. First, photo-ALE allows a submonolayer precision of material removal without the need to change the hardware that normally is required by the conventional ALE methods. Second, the photo-ALE process can be monitored in situ with either PL of a processed wafer or with the open-circuit potential of the photoetching material, as demonstrated by us recently.[36] Third, because the enhanced dissolution of the surface accumulating photo-ALE products is expected in the forced flow of a photocorroding liquid, a two-step etching cycle could be reduced below that of 25 s investigated in this report, which would result in a further accelerated photocorroding process. Our results demonstrate a relatively simple process for in situ diagnostics of ALE that could find application in the fabrication of compound semiconductor nanodevices and expand beyond merely topographical characterization of etched semiconductor surfaces.[64]

DOI: 10.1021/acsami.9b02079
ACS Appl. Mater. Interfaces 2019, 11, 17968−17978

■ ASSOCIATED CONTENT

Supporting Information

The Supporting Information is available free of charge on the ACS Publications website at DOI: 10.1021/acsami.9b02079.

PL spectroscopy at 20 K and during photo-ALE at 298 K (Wafer J0150); calculations of ions released from J0152 samples in DI H_2O and NH_4OH; dark corrosion data for J0152 in DI H_2O and NH_4OH; FTIR absorbance spectra of GaAs/AlGaAs (wafer J0152) photocorroded in DI H_2O; AFM 3D micrographs of J0152 samples; and advantages and disadvantages of representative digital etching methods of GaAs and GaAs/AlGaAs microstructures reported in the literature (PDF)

■ AUTHOR INFORMATION

Corresponding Author

*E-mail: jan.j.dubowski@usherbrooke.ca.

ORCID

Mohammad R. Aziziyan: 0000-0002-1698-7976

Jan J. Dubowski: 0000-0003-0022-527X

Author Contributions

The manuscript was written through contributions of all the authors. All the authors have given approval to the final version of the manuscript.

Funding

This research was supported by the Canada Research Chair in Quantum Semiconductors Program (grant no. 950-220304) and the Natural Sciences and Engineering Research Council of Canada (Discovery grant RGPIN-2015-04448 and Strategic Partnership grant SPG-2016-494057). One of the authors (MRA) acknowledges the support received in the frame of the NSERC-CREATE Training Program in Integrated Sensor Systems. The fabrication of GaAs/AlGaAs wafers was subsidized by the CMC Microsystems (Kingston, Canada).

Notes

The authors declare no competing financial interest.

■ ACKNOWLEDGMENTS

The authors are indebted to Dr. Khalid Moumanis for collecting wavelength-dependent PL spectra of the GaAs/AlGaAs wafers, Prof. Roland Leduc and Olivier Savary (Department of Civil Engineering, Faculty of Engineering, Université de Sherbrooke) for collecting ICP-MS data, and Sonia Blais (Centre de caractérisation des matériaux, Université de Sherbrooke) for collecting XPS data and assisting in their analysis.

■ REFERENCES

(1) Rosenberg, J. J.; Benlamri, M.; Kirchner, P. D.; Woodall, J. M.; Pettit, G. D. An $In_{0.15}Ga_{0.85}$ As/GaAs Pseudomorphic Single Quantum Well Hemt. *IEEE Electron Device Lett.* **1985**, *6*, 491−493.

(2) Smith, F. W.; Calawa, A. R.; Chen, C.-L.; Manfra, M. J.; Mahoney, L. J. New MBE Buffer Used to Eliminate Backgating in GaAs MESFETs. *IEEE Electron Device Lett.* **1988**, *9*, 77−80.

(3) Tsukamoto, S.; Nagamune, Y.; Nishioka, M.; Arakawa, Y. Fabrication of GaAs quantum wires on epitaxially grown V grooves by metal−organic chemical−vapor deposition. *J. Appl. Phys.* **1992**, *71*, 533−535.

(4) Dyer, G. C.; Aizin, G. R.; Allen, S. J.; Grine, A. D.; Bethke, D.; Reno, J. L.; Shaner, E. A. Induced Transparency by Coupling of Tamm and Defect States in Tunable Terahertz Plasmonic Crystals. *Nat. Photonics* **2013**, *7*, 925−930.

(5) Chen, S. S.; Lin, C. C.; Peng, C. K.; Chan, Y. J. Molecular Beam Epitaxy Regrowth and Device Performance of GaAs-Based Pseudomorphic High Electron Mobility Transistors Using a Thin Indium Passivation Layer. *J. Mater. Sci.: Mater. Electron.* **2000**, *11*, 483−487.

(6) Inoue, D.; Lee, J.; Hiratani, T.; Atsuji, Y.; Amemiya, T.; Nishiyama, N.; Arai, S. Sub-Milliampere Threshold Operation of Butt-Jointed Built-in Membrane DFB Laser Bonded on Si Substrate. *Opt. Express* **2015**, *23*, 7771−7778.

(7) Kosugi, T.; Iwase, H.; Gamo, K. Characteristics of Ion Beam Assisted Etching of GaAs: Surface Stoichiometry. *J. Vac. Sci. Technol., B: Microelectron. Nanometer Struct.–Process., Meas., Phenom.* **1993**, *11*, 2214−2218.

(8) Sugata, S.; Asakawa, K. Investigation of GaAs Surface Morphology Induced by Cl_2 Gas Reactive Ion Beam Etching. *Jpn. J. Appl. Phys.* **1983**, *22*, L813.

(9) Li, X.; Zhou, H.; Wilkinson, C. D. W.; Thayne, I. G. Optical Emission Spectrometry of Plasma in Low-Damage Sub-100 nm Tungsten Gate Reactive Ion Etching Process for Compound Semiconductor Transistors. *Jpn. J. Appl. Phys.* **2006**, *45*, 8364.

(10) Sugata, S.; Asakawa, K. GaAs Radical Etching with a Cl_2 Plasma in a Reactive Ion Beam Etching System. *Jpn. J. Appl. Phys.* **1984**, *23*, L564.

(11) Meguro, T.; Ishii, M.; Kodama, H.; Hamagaki, M.; Hara, T.; Yamamoto, Y.; Aoyagi, Y. Layer-by-Layer Controlled Digital Etching by Means of an Electron-Beam-Excited Plasma System. *Jpn. J. Appl. Phys.* **1990**, *29*, 2216.

(12) Maki, P. A.; Ehrlich, D. J. Laser Bilayer Etching of GaAs Surfaces. *Appl. Phys. Lett.* **1989**, *55*, 91−93.

(13) Dubowski, J. J.; Compaan, A.; Prasad, M. Laser-Assisted Dry Etching Ablation of InP. *Appl. Surf. Sci.* **1995**, *86*, 548−553.

(14) Kanarik, K. J.; Lill, T.; Hudson, E. A.; Sriraman, S.; Tan, S.; Marks, J.; Vahedi, V.; Gottscho, R. A. Overview of Atomic Layer Etching in the Semiconductor Industry. *J. Vac. Sci. Technol., A* **2015**, *33*, 020802.

(15) Mameli, A.; Verheijen, M. A.; Mackus, A. J. M.; Kessels, W. M. M.; Roozeboom, F. Isotropic Atomic Layer Etching of ZnO Using Acetylacetone and O_2 Plasma. *ACS Appl. Mater. Interfaces* **2018**, *10*, 38588−38595.

(16) Lee, Y.; DuMont, J. W.; George, S. M. Trimethylaluminum as the Metal Precursor for the Atomic Layer Etching of Al_2O_3 Using Sequential, Self-Limiting Thermal Reactions. *Chem. Mater.* **2016**, *28*, 2994−3003.

(17) Lee, Y.; George, S. M. Thermal Atomic Layer Etching of Titanium Nitride Using Sequential, Self-Limiting Reactions: Oxidation to TiO_2 and Fluorination to Volatile TiF_4. *Chem. Mater.* **2017**, *29*, 8202−8210.

(18) Abdulagatov, A. I.; George, S. M. Thermal Atomic Layer Etching of Silicon Using O2, HF, and $Al(CH_3)_3$ as the Reactants. *Chem. Mater.* **2018**, *30*, 8465−8475.

(19) Xie, W.; Lemaire, P. C.; Parsons, G. N. Thermally Driven Self-Limiting Atomic Layer Etching of Metallic Tungsten Using WF_6 and O_2. *ACS Appl. Mater. Interfaces* **2018**, *10*, 9147−9154.

(20) Johnson, N. R.; George, S. M. WO_3 and W Thermal Atomic Layer Etching Using "Conversion-Fluorination" and "Oxidation-Conversion-Fluorination" Mechanisms. *ACS Appl. Mater. Interfaces* **2017**, *9*, 34435−34447.

(21) DuMont, J. W.; Marquardt, A. E.; Cano, A. M.; George, S. M. Thermal Atomic Layer Etching of SiO_2 by a "Conversion-Etch" Mechanism Using Sequential Reactions of Trimethylaluminum and Hydrogen Fluoride. *ACS Appl. Mater. Interfaces* **2017**, *9*, 10296−10307.

(22) DeSalvo, G. C.; Bozada, C. A.; Ebel, J. L.; Look, D. C.; Barrette, J. P.; Cerny, C. L. A.; Dettmer, R. W.; Gillespie, J. K.; Havasy, C. K.; Jenkins, T. J.; Nakano, K.; Pettiford, C. I.; Quach, T. K.; Sewell, J. S.; Via, G. D. Wet Chemical Digital Etching of GaAs at Room Temperature. *J. Electrochem. Soc.* **1996**, *143*, 3652−3656.

(23) Ruberto, M. N.; Zhang, X.; Scarmozzino, R.; Willner, A. E.; Podlesnik, D. V.; Osgood, R. M., Jr. The Laser-Controlled

Micrometer-Scale Photoelectrochemical Etching of III−V Semiconductors. *J. Electrochem. Soc.* **1991**, *138*, 1174−1185.
(24) Willner, A. E.; Podlesnik, D. V.; Gilgen, H. H.; Osgood, R. M., Jr. Photobias Effect in Laser-Controlled Etching of InP. *Appl. Phys. Lett.* **1988**, *53*, 1198−1200.
(25) Kohl, P. A.; Ostermayer, F. W. J. Photoelectrochemical Methods for III-V Compound Semiconductor Device Processing. *Annu. Rev. Mater. Sci.* **1989**, *19*, 379−399.
(26) Fink, T.; Osgood, R. M. Photoelectrochemical Etching of GaAs/AlGaAS Multilayer Structures. *J. Electrochem. Soc.* **1993**, *140*, 2572−2581.
(27) Hennessy, K.; Badolato, A.; Tamboli, A.; Petroff, P. M.; Hu, E. Photonic Crystal Nanocavity Modes by Wet Chemical Digital Etching. *Appl. Phys. Lett.* **2005**, *87*, 021108.
(28) Lin, J.; Zhao, X.; Antoniadis, D. A.; del Alamo, J. A. A Novel Digital Etch Technique for Deeply Scaled III-V MOSFETs. *IEEE Electron Device Lett.* **2014**, *35*, 440−442.
(29) Shang, C. K.; Wang, V.; Chen, R.; Gupta, S.; Huang, Y.-C.; Pao, J. J.; Huo, Y.; Sanchez, E.; Kim, Y.; Kamins, T. I.; Harris, J. S. Dry-Wet Digital Etching of $Ge_{1-X}Sn_x$. *Appl. Phys. Lett.* **2016**, *108*, 063110.
(30) Shinoda, K.; Miyoshi, N.; Kobayashi, H.; Miura, M.; Kurihara, M.; Maeda, K.; Negishi, N.; Sonoda, Y.; Tanaka, M.; Yasui, N.; Izawa, M.; Ishii, Y.; Okuma, K.; Saldana, T.; Manos, J.; Ishikawa, K.; Hori, M. Selective Atomic-Level Etching Using Two Heating Procedures, Infrared Irradiation and Ion Bombardment, for Next-Generation Semiconductor Device Manufacturing. *J. Phys. D: Appl. Phys.* **2017**, *50*, 194001.
(31) Aziziyan, M. R.; Hassen, W. M.; Morris, D.; Frost, E. H.; Dubowski, J. J. Photonic Biosensor Based on Photocorrosion of GaAs/AlGaAs Quantum Heterostructures for Detection of *Legionella Pneumophila*. *Biointerphases* **2016**, *11*, 019301.
(32) Sharma, H.; Moumanis, K.; Dubowski, J. J. Ph-Dependent Photocorrosion of GaAs/AlGaAs Quantum Well Microstructures. *J. Phys. Chem. C* **2016**, *120*, 26129−26137.
(33) Aziziyan, M. R.; Hassen, W. M.; Dubowski, J. J. Electrically Biased GaAs/AlGaAs Heterostructures for Enhanced Detection of Bacteria. *Synthesis and Photonics of Nanoscale Materials XIII*, 2016, Vol. *9737*, pp 97370E1-97370E6.
(34) Nazemi, E.; Hassen, W. M.; Frost, E. H.; Dubowski, J. J., Monitoring growth and antibiotic susceptibility of Escherichia coli with photoluminescence of GaAs/AlGaAs quantum well microstructures. *Biosens. Bioelectron.* **2017**, *93*−240. DOI: 10.1016/j.bios.2016.08.112
(35) Aithal, S.; Liu, N.; Dubowski, J. J. Photocorrosion Metrology of Photoluminescence Emitting GaAs/AlGaAs Heterostructures. *J. Phys. D: Appl. Phys.* **2017**, *50*, 0351061−0351069.
(36) Aithal, S.; Dubowski, J. J. Open Circuit Potential Monitored Digital Photocorrosion of GaAs/AlGaAs Quantum Well Microstructures. *Appl. Phys. Lett.* **2018**, *112*, 1531021−1531025.
(37) Pröfrock, D.; Prange, A. Inductively Coupled Plasma-Mass Spectrometry (ICP-MS) for Quantitative Analysis in Environmental and Life Sciences: A Review of Challenges, Solutions, and Trends. *Appl. Spectrosc.* **2012**, *66*, 843−868.
(38) Sabine Becker, J.; Soman, R. S.; Becker, T.; Panday, V. K.; Dietze, H.-j. Trace and Ultratrace Analysis of Gallium Arsenide by Different Mass Spectrometric Techniques. *J. Anal. At. Spectrom.* **1998**, *13*, 983−987.
(39) Kyoung Jin, C.; Jae Kyoung, M.; Min, P.; Haechon, K.; Jong-Lam, L. Effects of Photowashing Treatment on Gate Leakage Current of GaAs Metal-Semiconductor Field-Effect Transistors. *Jpn. J. Appl. Phys.* **2002**, *41*, 2894.
(40) Passlack, M.; Hong, M.; Mannaerts, J. P.; Kwo, J. R.; Tu, L. W. Recombination velocity at oxide-GaAs interfaces fabricated by in situ molecular beam epitaxy. *Appl. Phys. Lett.* **1996**, *68*, 3605−3607.
(41) Joyce, H. J.; Docherty, C. J.; Gao, Q.; Tan, H. H.; Jagadish, C.; Lloyd-Hughes, J.; Herz, L. M.; Johnston, M. B. Electronic Properties of GaAs, InAs and InP Nanowires Studied by Terahertz Spectroscopy. *Nanotechnology* **2013**, *24*, 214006.
(42) Homma, Y.; Osaka, J.; Inoue, N. In situ Observation of Monolayer Steps During Molecular Beam Epitaxy of Gallium Arsenide by Scanning Electron Microscopy. *Jpn. J. Appl. Phys.* **1994**, *33*, L563.
(43) Lee, H.-Y. Growth of Gaas Oxide Layer Using Photoelectrochemical Method. *J. Electrochem. Soc.* **2008**, *155*, G141.
(44) Sutter, E. M. M.; Le Gall, M.; Debiemme-Chouvy, C. Behavior ofp-Type GaAs in an Aerated Boric Acid Solution at the Open-Circuit Potential. Influence of the Presence of Co(II) Ions. *J. Phys. Chem. B* **2001**, *105*, 4840−4845.
(45) Huang, Y.; Luo, J.; Ivey, D. G. Comparative Study of GaAs Corrosion in H_2SO_4 and $NH_3{\cdot}H_2O$ Solutions by Electrochemical Methods and Surface Analysis. *Mater. Chem. Phys.* **2005**, *93*, 429−442.
(46) Passlack, M.; Hong, M.; Schubert, E. F.; Kwo, J. R.; Mannaerts, J. P.; Chu, S. N. G.; Moriya, N.; Thiel, F. A. In Situ Fabricated Ga_2O_3−GaAs Structures with Low Interface Recombination Velocity. *Appl. Phys. Lett.* **1995**, *66*, 625−627.
(47) Liliental-Weber, Z.; Wilmsen, C. W.; Geib, K. M.; Kirchner, P. D.; Baker, J. M.; Woodall, J. M. Structure and Chemical Composition of Water-Grown Oxides of GaAs. *J. Appl. Phys.* **1990**, *67*, 1863−1867.
(48) Kauffman, J. F.; Richmond, G. L. Photoluminescence Enhancement Monitored in Real Time During Photowashing of GaAs. *Appl. Phys. Lett.* **1991**, *59*, 561−563.
(49) Clawson, A. R. Guide to references on III−V semiconductor chemical etching. *Mater. Sci. Eng., R* **2001**, *31*, 1−438.
(50) Schön, G. Auger and Direct Electron Spectra in X-Ray Photoelectron Studies of Zinc, Zinc Oxide, Gallium and Gallium Oxide. *J. Electron Spectrosc. Relat. Phenom.* **1973**, *2*, 75−86.
(51) Iwakuro, H.; Tatsuyama, C.; Ichimura, S. XPS and AES Studies on the Oxidation of Layered Semiconductor GaSe. *Jpn. J. Appl. Phys.* **1982**, *21*, 94.
(52) Procop, M. XPS Data for Sputter-Cleaned $In_{0.53}Ga_{0.47}As$, GaAs, and InAs Surfaces. *J. Electron Spectrosc. Relat. Phenom.* **1992**, *59*, R1−R10.
(53) Dua, A. K.; George, V. C.; Agarwala, R. P. Characterization and Microhardness Measurement of Electron-Beam-Evaporated Alumina Coatings. *Thin Solid Films* **1988**, *165*, 163−172.
(54) Wagner, C. D.; Passoja, D. E.; Hillery, H. F.; Kinisky, T. G.; Six, H. A.; Jansen, W. T.; Taylor, J. A. Auger and photoelectron line energy relationships in aluminum-oxygen and silicon-oxygen compounds. *J. Vac. Sci. Technol.* **1982**, *21*, 933−944.
(55) Kloprogge, J. T.; Duong, L. V.; Wood, B. J.; Frost, R. L. XPS Study of the Major Minerals in Bauxite: Gibbsite, Bayerite and (Pseudo-)Boehmite. *J. Colloid Interface Sci.* **2006**, *296*, 572−576.
(56) Takahashi, J. *Direct Measurement of Metallic Impurities in 20% Ammonium Hydroxide by Agilent 7700s ICP-MS*. Application Note from Agilent Technologies, 2011, Publication Number 5990-7914EN, pp 1−6.
(57) Pino, M.; Chacón, J.; Fatás, E.; Ocón, P. Performance of Commercial Aluminium Alloys as Anodes in Gelled Electrolyte Aluminium-Air Batteries. *J. Power Sources* **2015**, *299*, 195−201.
(58) Nelson, R. J.; Sobers, R. G. Interfacial Recombination Velocity in GaAlAs/GaAs Heterostructures. *Appl. Phys. Lett.* **1978**, *32*, 761−763.
(59) Tkachev, M.; Anand-Kumar, T.; Bitler, A.; Guliamov, R.; Naaman, R. Enabling Long-Term Operation of GaAs -Based Sensors in Aqueous Solutions. *Engineering* **2013**, *5*, 12.
(60) Downs, A. J. *Chemistry of Aluminium, Gallium, Indium and Thallium*, 1st ed.; Blackie Academic & Professional: London, 1993.
(61) Moon, E.-A.; Lee, J.-L.; Yoo, H. M. Selective Wet Etching of GaAs on $Al_xGa_{1-X}As$ for AlGaAs/InGaAs/AlGaAs Pseudomorphic High Electron Mobility Transistor. *J. Appl. Phys.* **1998**, *84*, 3933−3938.
(62) Karkare, S.; Bazarov, I. Effect of Nanoscale Surface Roughness on Transverse Energy Spread from GaAs Photocathodes. *Appl. Phys. Lett.* **2011**, *98*, 094104.

DOI: 10.1021/acsami.9b02079
ACS Appl. Mater. Interfaces 2019, 11, 17968−17978

(63) Akhundov, I. O.; Kazantsev, D. M.; Kozhuhov, A. S.; Alperovich, V. L. Optimization of Conditions for Thermal Smoothing GaAs Surfaces. *J. Phys.: Conf. Ser.* **2018**, *993*, 012010.
(64) Edwards, C.; Arbabi, A.; Popescu, G.; Goddard, L. L. Erratum: Optically monitoring and controlling nanoscale topography during semiconductor etching. *Light: Sci. Appl.* **2012**, *1*, No. e30.

DOI: 10.1021/acsami.9b02079
ACS Appl. Mater. Interfaces 2019, 11, 17968−17978